

The First Detection of [O IV] from an Ultraluminous X-ray Source with *Spitzer*. II. Evidence for High Luminosity in Holmberg II ULX

C. T. Berghea

Physics Department, The Catholic University of America, Washington, DC 20064

79berghea@cua.edu

R. P. Dudik

United States Naval Observatory, Washington, DC 20392

rpdudik@usno.navy.mil

K. A. Weaver and T. R. Kallman

Laboratory for High Energy Astrophysics, NASA Goddard Space Flight Center, Greenbelt, MD 20771

ABSTRACT

This is the second of two papers examining *Spitzer* Infrared Spectrograph (IRS) observations of the ultraluminous X-ray source (ULX) in Holmberg II. Here we perform detailed photoionization modeling of the infrared lines. Our analysis suggests that the luminosity and morphology of the [O IV] 25.89 μm emission line is consistent with photoionization by the soft X-ray and far ultraviolet (FUV) radiation from the accretion disk of the binary system and inconsistent with narrow beaming. We show that the emission nebula is matter-bounded both in the line of sight direction and to the east, and probably radiation-bounded to the west. A bolometric luminosity in excess of $10^{40} \text{ erg s}^{-1}$ would be needed to produce the measured [O IV] flux. We use modeling and previously published studies to conclude that shocks likely contribute very little, if at all, to the high-excitation line fluxes observed in the Holmberg II ULX. Additionally, we find that the spectral type of the companion star has a surprisingly strong effect on the predicted strength of the [O IV] emission. This finding could explain the origin of [O IV] in some starburst systems containing black hole binaries.

Subject headings: black hole physics — galaxies: individual (Holmberg II) — infrared: ISM — X-rays: binaries

1. INTRODUCTION

Despite over two decades of research (Fabbiano 1989), little is known about the intrinsic properties of ultraluminous X-ray sources (ULXs). They are characterized by extremely high X-ray luminosities, some reaching 10^{41} erg s $^{-1}$. These luminosities cannot be easily explained by normal stellar mass black hole systems, such as those found in our Galaxy. Beamed or super-Eddington stellar-mass systems have been presented as possible explanations for the extremely high X-ray luminosities in these objects. In addition, systems containing intermediate-mass black holes (IMBHs) are equally plausible sources for the emission. While these objects are easy to detect in the X-rays they are often faint or undetected in other energy bands, making them very difficult to characterize.

The ionization nebulae surrounding some ULXs have become critical for understanding the intrinsic properties of the central source, such as the intrinsic luminosity. For instance, Kaaret et al. (2004) (KWZ hereafter) and Pakull & Angebault (1986) have used the optical He II recombination line ($\lambda 4686$) to characterize the intrinsic X-ray luminosities of ULXs. However, we note that these and analogous studies are limited to the optical regime.

The very luminous ULX in the dwarf galaxy Holmberg II is one such object that has been studied extensively in both the X-ray and optical bands (Zezas et al. 1999; Lehmann et al. 2005; Goad et al. 2006; Abolmasov et al. 2007). It is located inside an ionized nebula (the “Foot nebula”), and shows high excitation optical emission lines coincident with the X-ray source (Pakull & Mirioni 2002; Abolmasov et al. 2007). The nebula appears to be perturbed by a moderate velocity field of ~ 50 km s $^{-1}$ (Lehmann et al. 2005). The optical counterpart of the ULX is a stellar-like bright source located in the “Heel” of the nebula, having emission consistent with a B supergiant to a main-sequence O star (Kaaret et al. 2004). Moreover, extended radio emission was detected, approximately coincident with the ionized nebula (Miller et al. 2005). The high excitation recombination line He II $\lambda 4686$ suggests photoionization by the ULX (KWZ), and the radio emission is inconsistent with emission from a SNR or an H II region.

In our first paper (Paper 1) we presented *Spitzer* Infrared Spectrograph (IRS) observations of the Foot nebula in Holmberg II. The low resolution spectral maps presented in that paper suggest that the high-ionization [O IV] line emission is coincident with the ULX position. Indeed we found the mid-IR line ratios for this object to be very similar to those seen in standard AGN (Genzel et al. 1998; Sturm et al. 2002; Dale et al. 2006). Our preliminary analysis suggested that [O IV], like the He II recombination line, can be used to constrain the spectral energy distribution (SED) of the ULX in both the UV and X-rays, thereby constraining the intrinsic X-ray luminosity. To this end, we presented archival X-ray, ultraviolet (UV) and infrared (IR) data and constructed a detailed SED of the ULX from

which photoionization models can be used break the degeneracy in X-ray models and extract a reliable bolometric luminosity for the source.

In this second paper we perform detailed photoionization modeling for the Holmberg II ULX. We use the spectral energy distribution (SED) obtained in Paper 1 as the ionizing source, and compare the predictions with the observed IR *Spitzer* spectrum. To better constrain the physical properties, we investigate how the predictions change when we vary the parameters: the accretion disk temperature, gas density, metallicity, and the stellar companion. We try both the radiation and matter-bounded geometries to explain the high and low-ionization IR lines. Finally, we explore shock models as a possible alternative to ionization. In Sections 5 and 6 we discuss our results and we present our conclusion.

2. Summary of Observational Results

The study of ULXs is limited almost exclusively to the X-ray band, where they appear very bright and uncontaminated. Studies of these objects at other wavelengths are difficult because the emission is generally either undetected or contaminated by circum-stellar or circum-nebular emission, making an estimate for the intrinsic bolometric luminosity very difficult. This deficiency, especially in the UV, results in degeneracy in X-ray models of the accretion process that cannot be broken. Our analysis of the X-ray emission from the ULX in Holmberg II is an example of such degeneracy. In Paper 1 three physically distinct models were presented to fit the X-ray spectra for the Holmberg II ULX. The resultant parameters from the fits are given in Table 1. Figures 1 - 3 show the spectra and the fitted components for all three models. A brief summary of the three models is as follows:

1. **Power-law Plus Multicolor Disk (PLMCD) Model:** This is a two-component model widely used to describe the emission from accreting black holes. As the name suggests, the model consists of a multi-color disk component and a power-law component for the hard tail. As discussed in Paper 1, when extrapolated to softer energies (the far UV) this model falls apart since the power law dominates in the UV. Indeed the model is unrealistic since it is physically impossible to have the X-ray photons Comptonized to lower energies. This model provides a good fit to the X-ray spectrum and is used extensively in other X-ray studies. However we emphasize that it is not physically meaningful. The PLMCD model is shown here as a base from which modified, but more physically meaningful models are derived.
2. **The Modified PLMCD Model:** The Modified PLMCD model is also a two-component model, but one for which the far-UV extrapolation is from the disk component rather

than the power-law component. This yields a much more physically meaningful interpretation for the emission.

3. **Broken Power Law (BPL) Model:** The spectra were also fit with a broken power-law model, which is much more flexible when extrapolated to the UV. Such a model would be produced if jet emission dominated the full SED.

As can be seen from Table 1, all three models provide reasonably good fits to the X-ray data. This degeneracy can only be broken through comprehensive knowledge of the shape of the UV continuum and detailed photoionization modeling of high-excitation lines. In the former case, the three X-ray models can be extrapolated to the UV and then compared with observational data. The best-fit extrapolated model to the UV spectrum provides some indication of the appropriate physical accretion scenario for the observational data. However, contamination to the UV emission by circum-stellar or circum-nebular continuum precludes a pure fit. Thus, in addition to this photometric data, high-excitation spectral lines, which require high-energy UV photons to ionize, can be used in combination with photoionization modeling to check the robustness of the fit. In Paper 1 we also presented multi-wavelength photometric data from archival *Spitzer*, *XMM-Newton* and *GALEX* observations of the Holmberg II ULX, and also *Hubble Space Telescope* and *Very Large Array* photometric data from the literature. These data were used to construct a detailed spectral energy distribution (SED) of the ULX (Fig. 4). All three X-ray models enumerated above are shown in the plot as dotted, thick solid, and dashed black lines respectively. The thick solid black line in Figure 4 represents the "base SED model" which is the input spectrum for the preliminary photoionization modeling explored below. As discussed in Paper 1 and shown in Figure 4, the Modified PLMCD model is chosen as the X-ray model for the base model, since it is the only extrapolated model that fits the optical and UV data well. Tables 1 and 2 provide the X-ray spectral fitting results and the IR line measurements from the first paper that will be the basis of the modeling in the current publication.

3. CLOUDY Modeling of the IR lines

To perform detailed photoionization modeling with CLOUDY¹, a number of input parameters need to be defined. Specifically, the geometry of the cloud needs to be described, the density and metallicity of the gas needs to be specified, and an input SED needs to be

¹Photoionization modeling was performed using version 07.02.01 of CLOUDY, described by Ferland et al. 1998.

established. The following outlines the specific input parameters used for the preliminary CLOUDY run. These parameters are later varied to check the final results.

1. **Gas Cloud Geometry:** The input geometry must describe the shape and thickness of the gas cloud. Shape includes, for example, a spherical, cylindrical, or plane-parallel geometry. The cloud thickness defines a radiation or matter bounded geometry. In their photoionization modeling, KWZ assumed a spherical geometry based on resolved optical lines, and assumed the nebula is radiation-bounded. However, they noted that the lower-ionization line [O I] is only detected west of the ULX, thereby suggesting a matter-bounded nebula in other directions. Though we also detected low-ionization lines in the IR spectrum (Table 2 in this paper and Figs. 1 and 2 in Paper 1), we begin with the spherical, radiation-bounded geometry in an attempt to reproduce the high-excitation [O IV] emission. We assume the inner radius of the cloud to be 0.1 pc, thus maximizing the ionizing flux. To constrain the size of the ionized nebula for the radiation bounded geometry, CLOUDY was run down to a temperature of 4000 K. At this temperature, the cloud thickness is 140 pc, and the column density is $4.2 \times 10^{21} \text{ cm}^{-2}$, more than ten times the X-ray estimated value.
2. **Density:** Density can be specified as varying, uniform or clumpy. In the preliminary CLOUDY model, we assume a constant gas density of 10 cm^{-3} as per KWZ and a filling factor of 1. This density was estimated by KWZ using the optical line surface brightness profiles predicted by CLOUDY.
3. **Metallicity:** Metallicity is expressed in terms of solar metallicities. We chose an input metallicity of $0.1 Z_{\odot}$, close to that of KWZ and Pilyugin et al. (2004).
4. **SED:** The input SED must specify the companion star and the X-ray model used to fit the UV to X-ray continuum. The input SED used in our preliminary analysis is described in Section 2 and results from the multi-wavelength photometric and spectroscopic observations presented in Paper 1. This so called "base SED model" utilizes the Modified PLMCD model, extrapolated to the UV. For the input SED we used a B2Ib supergiant spectrum to represent the stellar companion. The B2Ib supergiant was chosen because it better fits our UV data than the O5V (both are limits to the stellar spectral range suggested by KWZ). The bolometric luminosity of this model is $1.34 \times 10^{40} \text{ erg s}^{-1}$.

3.1. Results from the Base Model

The results of the first CLOUDY run, with the base models as the ionizing source, are given in Figure 5 (top-left panel), as the ratio of the predictions to the observed values. The CLOUDY model predicted values for the mid-IR lines are close to the observed values for the high ionization lines. A simple change to the base model such as a slightly younger companion star would be enough to fit the [O IV] line observed, as the analysis below indicates. We also show predictions for the He II flux measured by KWZ (2.7×10^{36} erg s⁻¹).

The low ionization lines are the most discrepant. This disparity between the model and the observations is likely caused by a matter-bounded geometry in at least some directions of the nebula, as already suggested by KWZ. However, many of the model parameters are not well known and we explore how changes to these can effect the line-flux predictions in the sections to follow.

We note that sensitivity and aperture effects could explain the discrepancy between the low ionization line fluxes predicted by the radiation-bounded base SED model and the observed values. Using the CLOUDY output we calculated surface brightness profiles expected for the mid-IR lines. CLOUDY predicts a spatial extent of 20 to 25 pc for the He II which is consistent with the findings of KWZ (15–26 pc). The [O IV] emission from the ULX should be extended to a radius of about ~ 20 pc according to the simulation. However, due to the poor resolution of our spectral maps (one LH pixel = 67.5 pc), it is unclear whether the model accurately predicts the spatial extent of the [O IV]. In addition, the CLOUDY models suggest that while sensitivity may have some effect on the observed low-ionization line fluxes, it is not solely responsible for the high predicted-to-observed line ratios for the radiation bounded base SED model.

3.2. Varying the X-ray Source Spectrum to the BPL and PLMCD models

We next tried changing the X-ray part of the source spectrum. We first replace the Modified PLMCD model with the PLMCD model described in Section 2, leaving the other CLOUDY parameters the same. The model is extrapolated to the edge of the [O IV] line where we introduce a break, so that it does not dominate the optical flux from the B2 star. Results from this CLOUDY simulation are shown in upper-right panel of Figure 5. The values predicted by this model are clearly not consistent with the measured values. This model predicts a strong [Ne V] line, which is not detected in our *Spitzer* observations, and a He II luminosity 27 times larger than measured by KWZ. The [O IV] flux predicted from this model is also an order of magnitude larger than the observed flux. We therefore rule

out this model as a good estimate for the X-ray source spectrum. We note that the PLMCD model has been used by many researchers to estimate disk temperatures and even black hole masses. Our findings imply that it is likely not an appropriate model for ULX high-energy spectra.

We then tried replacing the Modified PLMCD model with the BPL model described in Section 2. Here we found results similar to the PLMCD model, with [Ne V] predicted to be detected, and all the observed lines well overpredicted. We therefore conclude that neither the PLMCD model nor the BPL model with a radiation bounded geometry provide a good fit to the observed IR spectra. This was expected because both these models predict a very strong UV ionizing flux.

3.3. Varying Other Parameters

We investigate here in more detail how the strong radiation from the accretion disk photoionizes the surrounding ISM and produces the observed lines. Starting again with the base SED model in the radiation bounded geometry, we vary the input parameters to see how they affect the emitted spectrum. We first examine the dependence of the simulated line luminosities on the X-ray spectrum by changing the MCD disk temperature (kT_{in}), the gas density, metallicity and the inner radius of the cloud. Finally, we explore how the SED of the stellar companion affects the line luminosities. The models presented are based on the multi-wavelength data of the Holmberg II ULX and the known properties of the surrounding ISM, but this analysis can be applied to ULXs in general.

Varying the Disk Temperature: The disk temperature is first altered by shifting the X-ray base SED model to lower photon energies, such that the disk luminosity remains constant across the band. As can be seen from Figure 6a, when the disk component peaks at lower energies, the mid-IR emission lines become stronger. For cooler disks (0.1 keV) the [Ne V] line should be detected in our observations. In contrast, the lower ionization lines are not dependent on the disk temperature over the range usually found in ULXs (0.1–0.5 keV). We conclude from this that varying the disk temperature will not yield better results.

Varying the Gas Density of the Cloud: The results obtained by varying the density of the cloud are plotted in Figure 6b. The line luminosities are not particularly sensitive to gas density (see also KWZ), though the [O IV] luminosity increases slightly as the gas approaches the critical density. KWZ found that the He II line is clearly extended to 15–25 pc and consistent with a density of $\sim 10 \text{ cm}^{-3}$. We therefore conclude that varying the density of the gas will not do much to improve the model.

Varying the Metallicity: The dependence of the line luminosities on metallicity is shown in Figure 7a. The [O IV] and [Ne V] line dependence is linear. Interestingly, the base model with a higher input metallicity reproduces the measured [O IV] luminosity very well. In fact a metallicity of $0.19 Z_{\odot}$ (oxygen abundance of 9.3×10^{-5} in absolute value) reproduces the [O IV] to within the calibration error of the instrument, but without increasing the He II, which is already over-predicted in the current version of the model. We conclude from this that the input metallicity may be lower than it should be (see Pilyugin et al. 2004). However, we also note that a higher metallicity will predict higher fluxes for the low ionization lines, resulting in an even greater discrepancy for these lines.

Varying the Inner Radius of the Ionizing Cloud: Figure 7b shows that the ionizing power of the incident flux is diluted if the spherical cloud is too far away from the source. If the inner radius is larger than about 10–20 pc, the luminosities of the [O IV] and [Ne V] lines drop dramatically. Interestingly, the He II line, though similar to [O IV] in ionization potential, is nearly insensitive to the inner cloud radius. This is likely because the [O IV] and [Ne V] are in a higher stage of ionization than He II and as a result are much more affected by dilution of the ionizing photons (in other words a drop in the ionization parameter) from increasing the inner radius. We conclude from this that increasing the inner radius will only worsen our original results and will not affect the strength of the low ionization lines. Thus we conclude that the inner radius is likely close to the source as our original input parameter supposes.

Varying the Stellar Companion (the O5V star): To test the effect of the stellar companion on the IR lines we ran the base model with an O5V star replacing the B2Ib supergiant. The temperature and luminosity of the O5V star, 42000 K and 3.2×10^{39} erg s⁻¹, were chosen to match the model used by KWZ. The results (the lower-right panel of Fig. 5) show that the O5V star has a very strong impact on the high ionization lines. The luminosity of the [O IV] line increases by a factor of 3, and the [Ne V] line by factor of 2. If the companion is in fact an O5V star, our measured Optical Monitor (OM) and *GALEX* fluxes from Paper 1 are under-luminous and are likely affected by reddening. Inclusion of an O5V star also has a very different effect on the [O IV] versus the He II line. Indeed, the He II luminosity is predicted to increase by only 11%. The strong impact of the O5V star can be explained if the O star produces copious O⁺⁺ ions (i.p. 35 eV), which are in turn ionized further by the ULX. The O star thus acts as a catalyst to the higher-energy photons from the ULX. A comparison between the oxygen ions structure for these models is presented in Figure 8a. The number of photons in the 24.6–54.4 eV interval is three times higher for the O5V star (7.27×10^{48} s⁻¹ compared to 2.42×10^{48} s⁻¹) than the B2Ib supergiant. Figure 8b shows that the local cloud temperature for the O5V star is also about two times higher in the region where the O³⁺ ions are produced (at offsets of 10–20 pc). Indeed, the [O III] $\lambda 5007$ luminosity estimated

from CLOUDY increases by a factor of six when the O5V star is used instead of the B2Ib supergiant.

The companion star therefore has an indirect but strong impact on the [O IV] line emission. A similar effect can be seen on a smaller scale for the [Ne V] line, which has an even higher ionization potential (97 eV). Thus, the [O IV] line does not act simply as a high energy photon counter as is the case with the He II line, but can also provide information about abundances of lower energy photons. This effect can be used to explain the detection of [O IV] in star-forming regions. In this scenario, [O IV] can be produced by relatively faint sources of soft X-rays and UV photons hidden in the star forming region, including such sources as ULXs, X-ray binaries, or SNR. This is a significant result, since the origin of [O IV] in star forming galaxies has been the subject of debate in the literature (Lutz et al. 1998; Schaerer & Stasińska 1999). Finally we conclude that an O5 star is likely not the companion star for the Holmberg II ULX. However later-type stars (but those earlier than a B2Ib supergiant), such as an O8 star, might better predict the [OIV] flux in the base model.

3.4. Varying the Geometry

As mentioned at the beginning of this section, KWZ found evidence from low-ionization optical lines that the ionized nebula is matter-bounded, at least in the east. This is also suggested by the IR line maps presented in Paper 1 and by the over-prediction of the low-ionization lines by the radiation bounded base SED model above. We also noticed that the absorption suggested by the X-ray spectrum is too low compared to that implied by a radiation-bounded geometry. More precisely, for our base SED model, the simulation requires a column density of $4.2 \times 10^{21} \text{ cm}^{-2}$, which is more than ten times larger than the measured values from spectral fits (see also the beginning of this section). This suggests that the nebula is also matter-bounded in the line-of-sight direction.

To simulate a matter-bounded geometry, we first ran the base SED model with the geometry described by a spherical cloud of varying thickness, so that the total hydrogen column ranges between 10^{20} and 10^{22} cm^{-2} . These results are plotted in Figure 9a. The column obtained from the X-ray fit is shown as a vertical line and labeled “Matter Bounded”. For this value, the predicted fluxes for both [O IV] and He II lines are much lower than the observed values. Therefore, this simple matter bounded geometry using the base SED model is not sufficient to reproduce the observed lines. As Figure 9a shows, the minimum column density required for the base model to predict the measured values for the high excitation lines is $\sim 5 \times 10^{20}$, or a cloud thickness of 16 pc (the dashed vertical line). This 16 pc is within the 15-25 pc radii observed in the He II emission line maps from KWZ. Therefore the

matter bounded case could work, if the observed X-ray column density were slightly higher than the X-ray predicted value of 3.26×10^{20} .

We next replaced the Modified PLMCD model for the BPL model as the X-ray fit for the SED. The broken power-law model is better suited than the Modified PLMCD model to test the matter bounded geometry. By varying this absorption parameter in the model within the errors allowed by the fit, we obtained a family of broken-power models, all consistent with the X-ray data, but predicting very different slopes in the ionizing part of the SED (the photon index varies between 1.3 and 2.2). A subset of the broken power-law models are shown in Figure 4. We re-ran our CLOUDY simulation for these models with the corresponding column densities from the X-ray fits. The results are plotted in Figure 9b. The best fit broken power-law X-ray model (BPL) is shown as a vertical line in this figure. The predicted line luminosities for this model are given in the lower-left panel of Figure 5.

As was the case with the original, radiation bounded base SED model, the predictions are very good for the high-ionization lines. The cloud radius is 17.7 pc, which is consistent with the size of the nebula found by KWZ in the east and south. However, contrary to the original radiation-bounded base model, the ULX makes no contribution to the low-ionization lines. This is true even for the largest column density, $9.2 \times 10^{20} \text{ cm}^{-2}$ (a 29.7 pc cloud radius for a gas density of 10 cm^{-3}). However, the spectral maps in Figure 3 of Paper 1 show that the ULX is likely to contribute at least to [Ne III] and probably [Si II].

Thus we conclude that the matter-bounded geometry alone does not fit all of the mid-IR spectral observations well. In fact, these results suggest that the geometry is complicated, being asymmetric and including both radiation and matter bounded geometries. KWZ found similar results. They find that to the south and east, He II and $\text{H}\beta$ emission suggests a matter-bounded geometry: the low excitation lines are absent here but detected in the west at larger offsets. Our CUBISM maps from Paper 1 suggest something similar, though the spatial resolution here is limited compared with the *HST* observation. The fact that the low-ionization line luminosities predicted by the matter-bounded models are much lower than the ones predicted by the radiation-bounded geometry suggests that a combination of the two geometries would yield predicted values that are very close to the observations.

4. Shock Models

The radiation-bounded/matter-bounded geometric scenario presented in Section 3 to explain the mid-IR line fluxes in the Holmberg II ULX presumes photoionization as the source of the line emission. However, shocks could also produce such lines. Indeed, a combination

of X-ray photoionization and shocks was recently proposed to explain the morphology of optical lines observed in the vicinity of LMC X-1 (Cooke et al. 2007). In this case the shocks are likely driven by a jet. Abolmasov et al. (2007) performed optical spectroscopy on eight ULXs with nebular counterparts, including the Holmberg II ULX, and found evidence for shocks in all cases based on the $[\text{S II}] \lambda\lambda 6717, 6731/\text{H}\alpha$ ratio. However, using high-excitation lines such as He II and $[\text{O III}]$, these authors also found that Holmberg II ULX and three other ULXs required photoionization to sufficiently explain the optical ratios.

Lehmann et al. (2005) found evidence of radial velocity variations of $\pm 50 \text{ km s}^{-1}$ from a region similar of size to the He III nebula. It is therefore possible that part of the ionization is caused by shocks. Lutz et al. (1998) suggested that velocity shocks of $100\text{--}200 \text{ km s}^{-1}$ can produce significant $[\text{O IV}]$ emission. However, when we also take into account the optical data, and in particular the detection of the He II recombination line, our data provide strong evidence *against* shocks as the source of the $[\text{O IV}]$ emission. This is primarily because the He II is not easily produced by shocks. Instead, the simultaneous detection of these lines argues for the presence of significant radiation over the He II edge (see also Schaerer & Stasińska 1999), and therefore suggests photoionization as the most likely line production mechanism.

Nevertheless, we checked to see if shock models could explain the mid-IR line luminosities and ratios observed in Holmberg II. We used Mappings III grids from Allen et al. (2008) to construct diagnostic diagrams. The predicted $[\text{O IV}]$ emission from shocks is shown in Figure 10a. We show both pure shocks and shocks with ionized precursors at a gas density of 1 cm^{-3} , and metallicity $0.1 Z_{\odot}$. For these models, the parameters varied are the shock velocity and the “magnetic parameter” $B/n^{1/2}$, where B is the magnetic field and n is the gas density (Dopita & Sutherland 1996).

The CUBISM measured fluxes from the brightest and faintest pixels in the $[\text{O IV}]$ map (yellow and blue pixels in Fig. 3 of Paper 1, respectively) are shown as horizontal lines in Figure 10a. We note that the maximum intensity of the line is likely higher than these levels. Indeed the $[\text{O IV}]$ emission is not spatially resolved and the plotted levels are actually averages over the size of the LH pixel (67.5 pc), rather than the maximum from each of the averaged slits. In spite of this, the levels plotted in Figure 10a requires significant shock velocities and such velocities ($> 200 \text{ km s}^{-1}$) were not detected by Lehmann et al. (2005).

For optical lines we chose the He II and the $[\text{O III}] \lambda\lambda 4363, 5007$ lines, as per Evans et al. (1999). The ratio $[\text{O III}] \lambda 4363 / [\text{O III}] \lambda 5007$ is sensitive to the gas temperature. Using the data from Lehmann et al. (2005) we calculated the ratio $([\text{O III}] \lambda 4959 + [\text{O III}] \lambda 5007) / [\text{O III}] \lambda 4363 = 50$, and estimate a temperature of 17800 K (Osterbrock & Ferland 2006). This is consistent with the temperature of the gas in the region of the cloud where

O^{++} ions are produced (see Fig. 8b). For the He II/ $H\beta$ ratio we chose an average (0.2) between the measurements of KWZ, Pakull & Mirioni (2002), and Lehmann et al. (2005). The shock grids for the optical lines are plotted in Figure 10b. For comparison, we overplotted the published data for two other ULXs with detected nebulae, Holmberg IX ULX and MF16 in NGC 6946 (Abolmasov et al. 2007). While the Holmberg IX ULX data is consistent with shocks with modest velocities ($< 100 \text{ km s}^{-1}$), Holmberg II ULX and MF16 seem to require very high velocities. Even for the shock plus precursor models, velocities in excess of 300 km s^{-1} are required to reproduce the observed line ratios and Lehmann et al. (2005) find velocities of only 50 km s^{-1} .

In summary, some contribution from shocks to the high excitation lines detected from Holmberg II ULX cannot be ruled out completely. However, if there is some contribution from shocks to the high ionization emission line luminosities, it is likely very small, since both He II and [O IV] lines require shocks with velocities in excess of 200 km s^{-1} , and such velocities were not seen by Lehmann et al. (2005).

5. Discussion of the Modeling Results

We find that the *Spitzer* observations of the Holmberg II ULX and especially the detection of the [O IV] line is consistent with photoionization by radiation from the ULX. Of all the lines examined, only the [O IV] line is shown to be clearly correlated with the ULX. However, some contribution by the ULX to the [Si II], [S III] and [Ne III] emission line flux is also likely. A summary of our main results is given below.

1. **The Base Model (Modified PLMCD):** The CLOUDY simulations show that the *Spitzer* spectrum is consistent with photoionization by the accretion powered emission from the ULX. We find that limited sensitivity might explain the relatively low fluxes observed for some low-ionization lines. The base SED model predicts a slightly lower [O IV] luminosity than the measured values for the radiation bounded case (Fig. 5), and even lower for the matter-bounded case (Figure 9a). Previous X-ray results have shown that the accretion disk temperature is likely lower than in our base model (KWZ obtained $\sim 0.2 \text{ keV}$). Such a disk temperature will increase the predicted line luminosity to match our measurements (Fig. 6a). A slightly higher metallicity ($0.2 Z_{\odot}$) can yield better fits to both the [O IV] and He II data for this base model. This is because the He II line is already over-predicted and raising the metallicity will not increase this discrepancy (Fig. 7a). In support of this, a metallicity of 0.17 was measured by Pilyugin et al. (2004). We note that while this model reproduces the spectra very well, it requires absorbing columns in the X-rays that are inconsistent with the observations.

2. **The PLMCD Model:** We find that the widely used PLMCD model, when extrapolated to the UV, is *not* consistent with the observations. The high excitation lines predicted using this model are at least ten times larger than observed. In this case lowering the metallicity to match the [O IV] will not work, because He II will still be much over-predicted. This model has been used extensively to model the X-ray data from ULXs, and sometimes used to find evidence for IMBHs (“cool disks” Miller et al. 2004). More recently this model has been used with more caution (Berghea et al. 2008), but we have shown that this model is inconsistent with the *Spitzer* observations of the Holmberg II ULX.
3. **Matter vs. Radiation Bounded Geometry:** The intensity and morphology of the IR lines provides spatial information about the emission line nebula around the Holmberg II ULX. The geometry consistent with our infrared data (and previously published optical data) is approximately spherical but not symmetrical. The CUBISM maps show that to the east and south the nebula shows only high excitation lines that are likely matter-bounded, while in the west, the detection of lower excitation lines might suggest a radiation-bounded cloud. However, observational effects, such as aperture and sensitivity effects, preclude any definitive conclusion on this model. The discrepancies found in Section 3.1 between the CLOUDY model and the measured values for the low-excitation lines suggest that the matter-bounded geometry is at play at least in part (probably to east and south as found from the spectral maps). Moreover, the absorption measurements from the X-ray data require the cloud to be at least matter-bounded toward our line of sight. Therefore, we find that both matter bounded and radiation bounded geometries are likely at work to describe the observed spectra in both the Mid-IR and X-rays.
4. **Shock Models:** The shocks models for both IR and optical emission lines show that shocks with velocity $>200 \text{ km s}^{-1}$ are required to generate both the He II and [O IV] lines observed in Holmberg II. The detected radial velocity variations around the ULX are of the order of $\pm 50 \text{ km s}^{-1}$ (Lehmann et al. 2005). Contribution from shocks to these lines is therefore likely to be small.
5. **True X-ray Luminosity:** The ULX luminosity estimated using photoionization modeling is independent of the estimate based on the X-ray flux, which can be affected by both absorption and beaming (King et al. 2001). The nebular emission line luminosities, on the other hand, are time-averaged true luminosities and can provide information about the geometry of emission and the surrounding ISM.

It is now widely accepted that ULXs are variable on timescales from days to years. These timescales are much shorter than the ionization equilibrium timescales in the

nebula. Chiang & Rappaport (1996) investigated time-dependent photoionization of H and He for supersoft X-ray sources. The He II ionization equilibrium at the 90% level is reached in $\sim 0.7 \tau_R$ after source turn-on, where $\tau_R = 3000$ yr is the recombination time for He^{++} from KWZ. For periodic sources, it was found that the He II line luminosity decreases significantly with increasing source period. For example, for a period of $10 \tau_R$ and a duty cycle of 10%, the estimated luminosity is 4.7% of that expected from a steady source with the same peak luminosity. That is a 53% deviation from a linear scaling law (10% of the steady state). This implies that if the Holmberg II ULX is variable, the estimates of KWZ based on the He II line are actually lower limits of the time-averaged luminosity.

For O^{+3} , the recombination time is shorter, $\tau_R \approx 100$ yr (Osterbrock & Ferland 2006), for the same ionization conditions: electron density 10 cm^{-3} and temperature 20000 K. We expect therefore that the [O IV] line reaches equilibrium in a shorter time (< 100 yr), but still long enough to provide a time-averaged estimate of the true luminosity of the ULX over $\sim 10 - 100$ yr. We note that light travel time (53 yr for a O^{+3} nebula of 16 pc), is an important factor in this case, because it is comparable to the recombination time.

Finally, the morphology of the emission lines, from both the previously published optical data and our IR data suggest emission that is nearly isotropic, being inconsistent with narrow beaming. Moreover, photoionization modeling with our base model is consistent with the detected high ionization lines, the true bolometric luminosity of this model is $> 10^{40} \text{ erg s}^{-1}$. This is well above the Eddington luminosity for a stellar-mass BH. In addition, some observational results indicate that the BH in Holmberg II is likely much larger than a stellar mass black hole (see description below).

6. **Impact on IR Studies of Starbursts:** We find that the predicted [O IV] line luminosity is significantly affected by the type of the companion star. Faint [O IV] has been detected in many starbursts and star-forming regions, but its origin is still under debate. Our analysis provides some explanation for this emission, suggesting that the [O IV] line could be produced by relatively faint X-ray sources including X-ray binaries, SNR or ULXs in starburst galaxies.

6. Conclusion

The bolometric luminosity of the base model is $1.33 \times 10^{40} \text{ erg s}^{-1}$. For accretion within the Eddington limit, the mass of the central BH is at least $85 M_\odot$. The estimate based on the inner disk temperature (0.38 keV) in the MCD model gives a much larger mass, $994 M_\odot$.

Finally, scaling from AGN estimates, the [O IV] emission predicts a mass as large as $10^4 M_{\odot}$. While our analysis excludes strong beaming in Holmberg II ULX, a sub-Eddington IMBH or a super-Eddington stellar-mass BH are both plausible ionization mechanisms that stem from our analysis. Given the X-ray spectral analysis in the literature, and our results that suggest that the ULX has maintained a high luminosity over timescales > 100 yr, we prefer the IMBH scenario. However, our CLOUDY modeling results alone cannot discriminate between these two sources or the two black hole estimates, since we have no way of constraining the accretion rate.

C. T. B. thanks Richard Mushotzky and Lisa Winter for helpful discussions, and Nicholas Sterling and Marcio Meléndez for their help with CLOUDY. R. P. D. gratefully acknowledges financial support from the NASA Graduate Student Research Program. This work is based on observations made with the Spitzer Space Telescope, which is operated by the Jet Propulsion Laboratory, California Institute of Technology under a contract with NASA. We thank the referee for very helpful and constructive comments that have significantly improved this paper.

REFERENCES

- Abolmasov, P., Fabrika, S., Sholukhova, O., & Afanasiev, V. 2007, *Astrophysical Bulletin*, 62, 36
- Allen, M. G., Groves, B. A., Dopita, M. A., Sutherland, R. S., & Kewley, L. J. 2008, *ApJS*, 178, 20
- Berghea, C. T., Weaver, K. A., Colbert, E. J. M., & Roberts, T. P. 2008, *ApJ*, 687, 471
- Chiang, E., & Rappaport, S. 1996, *ApJ*, 469, 255
- Cooke, R., Kuncic, Z., Sharp, R., & Bland-Hawthorn, J. 2007, *ApJ*, 667, L163
- Dale, D. A., et al. 2006, *ApJ*, 646, 161
- Dopita, M. A., & Sutherland, R. S. 1996, *ApJS*, 102, 161
- Evans, I., Koratkar, A., Allen, M., Dopita, M., & Tsvetanov, Z. 1999, *ApJ*, 521, 531
- Fabbiano, G. 1989, *ARA&A*, 27, 87
- Genzel et al. 1998, *ApJ*, 498, 579

- Goad, M. R., Roberts, T. P., Reeves, J. N., & Uttley, P. 2006, MNRAS, 365, 191
- Kaaret, P., Ward, M., & Zezas, A. 2004, MNRAS, 351, L83
- King, A. R., Davies, M. B., Ward, M. J., Fabbiano, G., & Elvis, M. 2001, ApJ, 552, L109
- Lehmann, I. et al. 2005, A&A, 431, 847
- Lutz, D., Kunze, D., Spoon, H. W. W., & Thornley, M. D. 1998, A&A, 333, L75
- Miller, J. M., Fabian, A. C., & Miller, M. C. 2004, ApJ, 614, L117
- Miller, N. A., Mushotzky, R. F., & Neff, S. G. 2005, ApJ, 623, L109
- Mitsuda, K. et al. 1984, PASJ, 36, 741
- Miyaji, T., Lehmann, I., & Hasinger, G. 2001, AJ, 121, 3041
- Osterbrock D. & Ferland G., Astrophysics of Gaseous Nebulae and active Galactic Nuclei, Second Edition, 2006, University Science Books, Sausalito, California.
- Pakull, M., & Mirioni, L. 2002, in “New Visions of the X-ray Universe in the XMM-Newton and Chandra Era”, (Noordwijk: ESTEC), (astro-ph/0202488)
- Pilyugin, L. S., Vílchez, J. M., & Contini, T. 2004, A&A, 425, 849
- Schaerer, D., & Stasińska, G. 1999, A&A, 345, L17
- Sturm, E., Lutz, D., Verma, A., Netzer, H., Sternberg, A., Moorwood, A. F. M., Oliva, E., & Genzel, R. 2002, A&A, 393, 821
- Zezas, A. L., Georgantopoulos, I., & Ward, M. J. 1999, MNRAS, 308, 302

Table 1. X-ray model fits

Model (1)	N_H (2) (10^{20} cm^{-2})	kT_{in}/Γ_1 (3) (keV)	Γ/Γ_2 (4)	$\Delta\chi^2/\text{dof}$ (5)	L (6) ($10^{40} \text{ erg s}^{-1}$)	MCD flux (7)
Modified PLMCD	3.26 ± 0.56	0.38 ± 0.02	2.54 ± 0.02	1.02/135, 0.974/713	1.11	0.49
PLMCD	10.4 ± 0.70	0.27 ± 0.02	2.42 ± 0.05	1.1386/849	2.28	0.12
BPL	5.49 ± 0.78	1.73 ± 0.10	2.57 ± 0.02	1.0316/849	1.41	0.60

Note. — (1): X-ray model, as described in Section 2. (2): Intrinsic hydrogen column density. The Galactic column density from KWZ ($3.42 \times 10^{20} \text{ cm}^{-2}$) was added separately. (3): Inner disk temperature for the MCD component. For the broken power-law model (BPL), this is the first (low energies) photon index parameter. The break is at 1.0 keV. (4): Photon index for the power-law component. For the broken power-law model this is the second (high energies) photon index parameter. (5): Reduced χ^2 values for the fit and the number of degrees of freedom. For the Modified PLMCD model, we quote two values for each separately fitted component (see text for details). (6): Unabsorbed (intrinsic) luminosities between 0.1 and 10 keV. (7): MCD component unabsorbed flux as fraction of the total flux for the PLMCD model. For the other two models, this simply the ratio of the flux between 0.1 and 1.0 keV to the flux in the whole range (0.1–10 keV)

Table 2. Measured infrared lines

Line (1)	Standard Aperture			Small Aperture		
	Flux (2)	S/N Ratio (3)	L (4)	Flux (5)	S/N Ratio (6)	L (7)
[Ne II] 12.81 μm	<6.08	...	<0.68	<1.98	...	<0.22
[Ne III] 15.56 μm	12.15 ± 3.4	4.60	1.35 ± 0.39	5.46 ± 1.37	7.6	0.61 ± 0.15
[S III] 18.71 μm	2.64 ± 1.14	4.64	0.29 ± 0.13	3.02 ± 1.16	4.7	0.34 ± 0.13
[Ne V] 24.32 μm	<3.88	...	<0.43	<1.16	...	<0.13
[O IV] 25.89 μm	7.01 ± 1.60	10.16	0.78 ± 0.2	3.63 ± 0.91	44.4	0.40 ± 0.1
[S III] 33.48 μm	<4.39	...	<0.49	<1.53	...	<0.17
[Si II] 34.82 μm	21.91 ± 5.48	9.90	2.44 ± 0.61	5.87 ± 1.47	7.2	0.65 ± 0.16

Note. — We show line fluxes for the standard (slightly smaller than the SH map) and the small aperture (4 LH pixels) as defined in Section 2 of Paper 1. Fluxes are in $10^{-22} \text{ W cm}^{-2}$, luminosities (L) in $10^{37} \text{ erg s}^{-1}$. If the measurements errors are smaller than the absolute calibration accuracy of 25%, the latter were used. For nondetections we show 3σ upper limits.

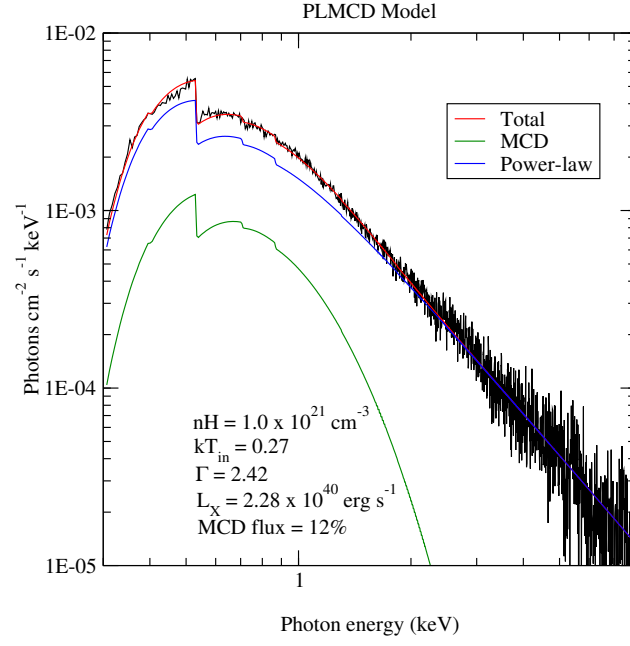


Fig. 1.— PLMCD model fit to the *XMM-Newton* spectrum. This is the typical model used for ULXs: a multi-colour disk component (MCD) plus a power-law at high energies.

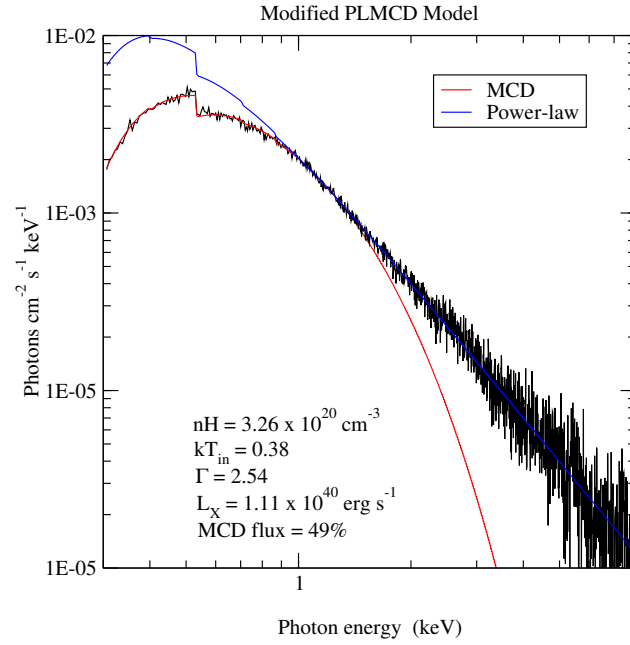


Fig. 2.— The Modified PLMCD model fit. Here the MCD component and the power-law are fitted separately below and above 1 keV, respectively.

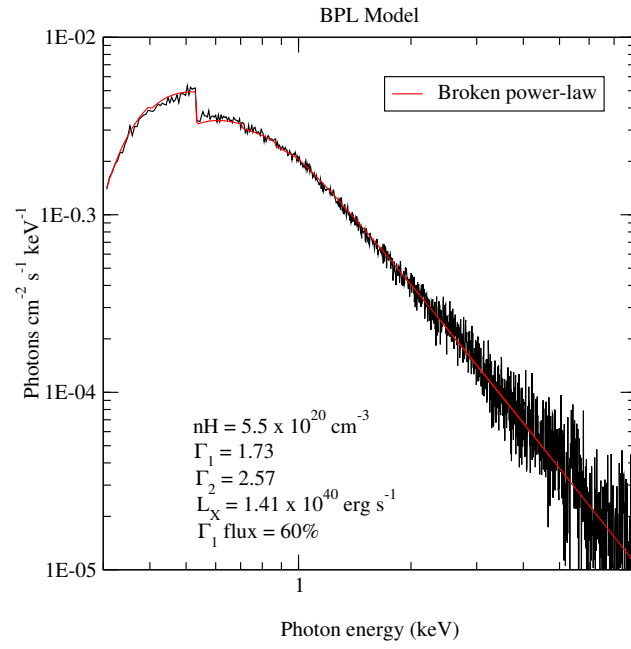


Fig. 3.— The broken power-law model fit. The break is at 1 keV, the same energy where the two components are separated in the Modified PLMCD model in Fig. 2.

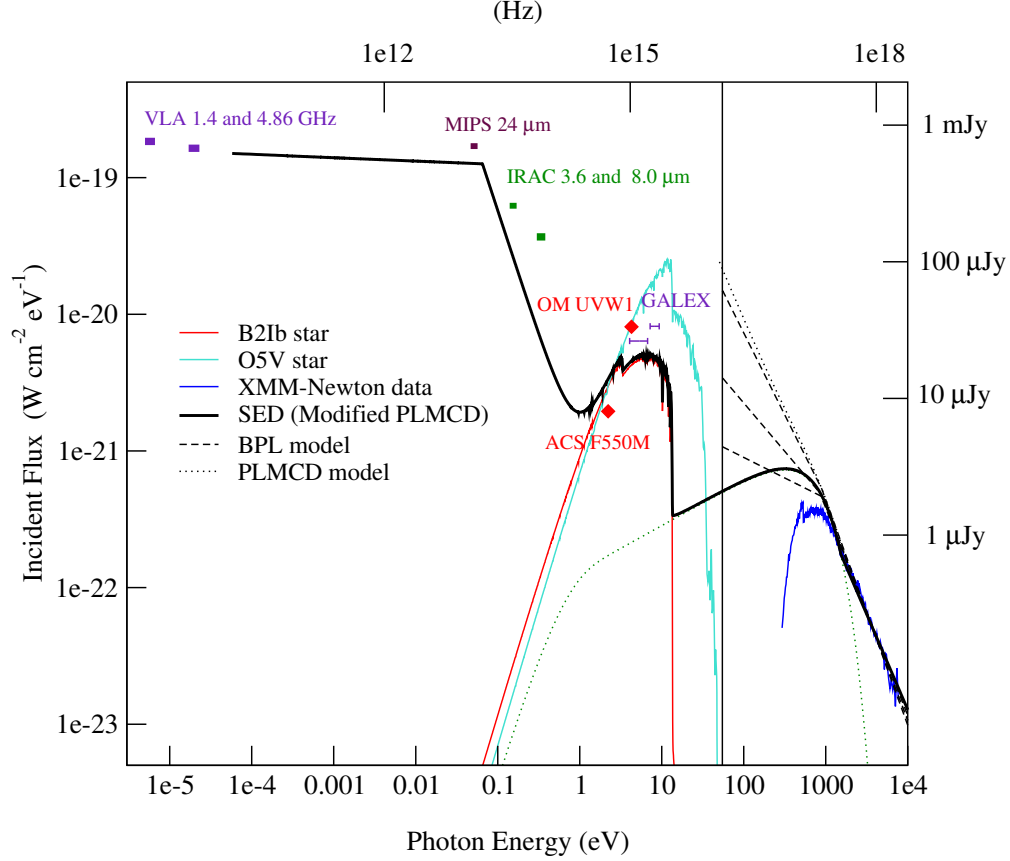


Fig. 4.— The input SED (Base model) constructed in Paper 1 and used as ionizing source in CLOUDY. The radio data is from Miller et al. (2005), the V-band magnitude for the optical counterpart of the ULX is quoted from KWZ. Our measured fluxes in Paper 1 using IRAC, MIPS, OM and *GALEX* are upper bounds, and therefore our model is below these data points. The two stellar spectra correspond to the spectral types range consistent with the colors and magnitudes in KWZ. The three models fit to the X-ray data are shown, extrapolated to the [O IV] edge at 54.93 eV (shown as a vertical line). The BPL model was used to obtain a family of broken power-law models, all compatible with the X-ray data within the errors. We show the lower and upper limits of this family as the lower and upper dashed lines, corresponding to $\Gamma = 1.3$ and $\Gamma = 2.2$ in the low energy slope, respectively. The middle dashed line represents the best fit BPL model shown in Table 1. The SED is constructed using the preferred X-ray model, Modified PLMCD.

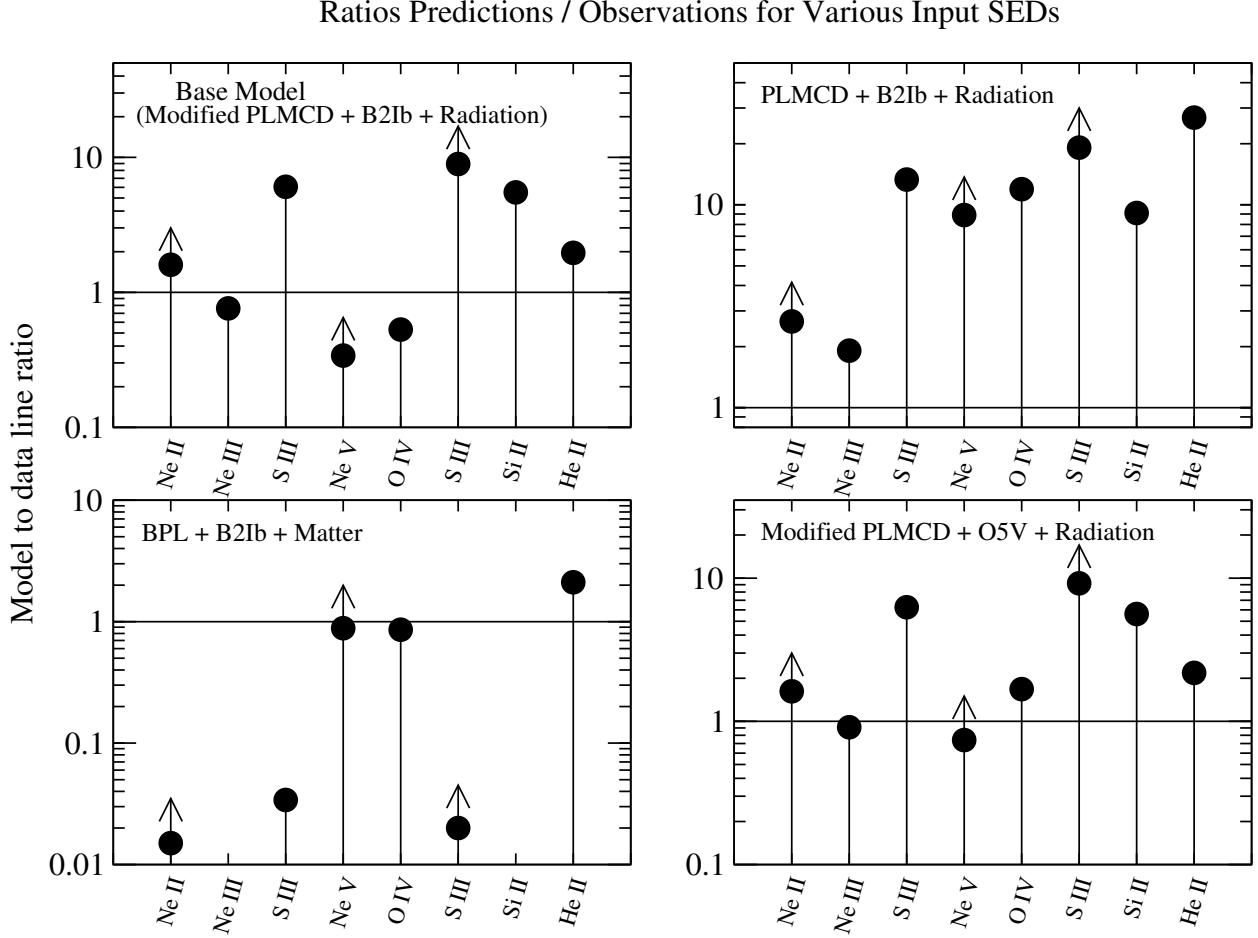


Fig. 5.— We show predictions for the IR lines from the CLOUDY modeling for various ionizing SEDs. We also included the He II $\lambda 4686$ line measured by KWZ (2.7×10^{36} erg s $^{-1}$). They are presented as model-to-data flux ratios. For non-detected lines, the plotted values are lower limits and are marked with an arrow pointed upward. The predictions for the [Ne III] and [Si II] lines are < 0.01 in the BPL model (lower-left) and are not shown. The perfect match line (ratio = 1) is shown on all plots. The errors are small, similar in size to the data points, therefore are not shown. The measured line fluxes are presented in the Table 2.

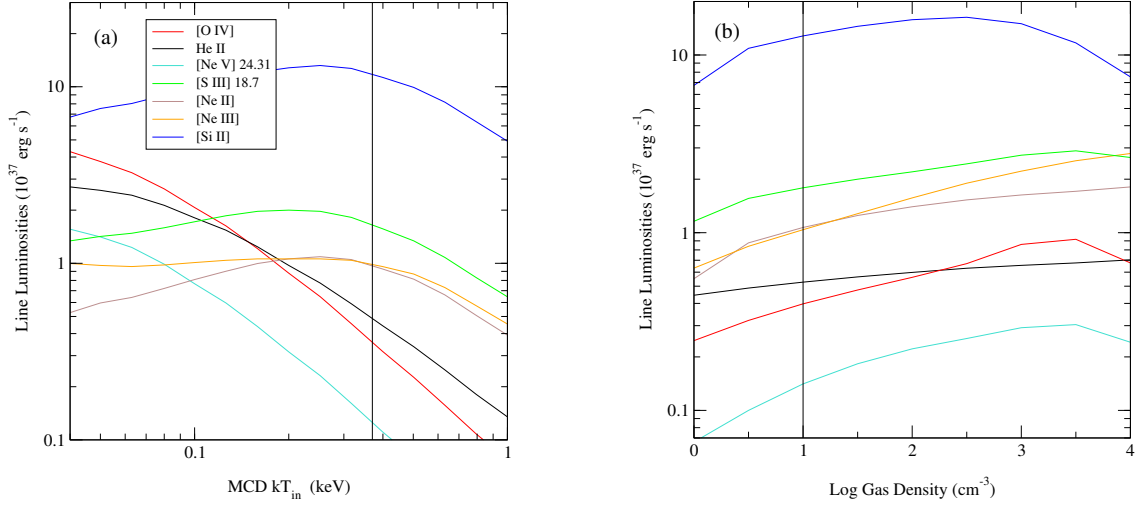


Fig. 6.— The dependence of the simulated lines from CLOUDY on: a) MCD inner disk temperature. b) Gas density of the cloud. The vertical lines mark the base model values: $kT_{in} = 0.38$ keV, density = 10 cm^{-3} . The line colors are the same but only labeled in the left panel.

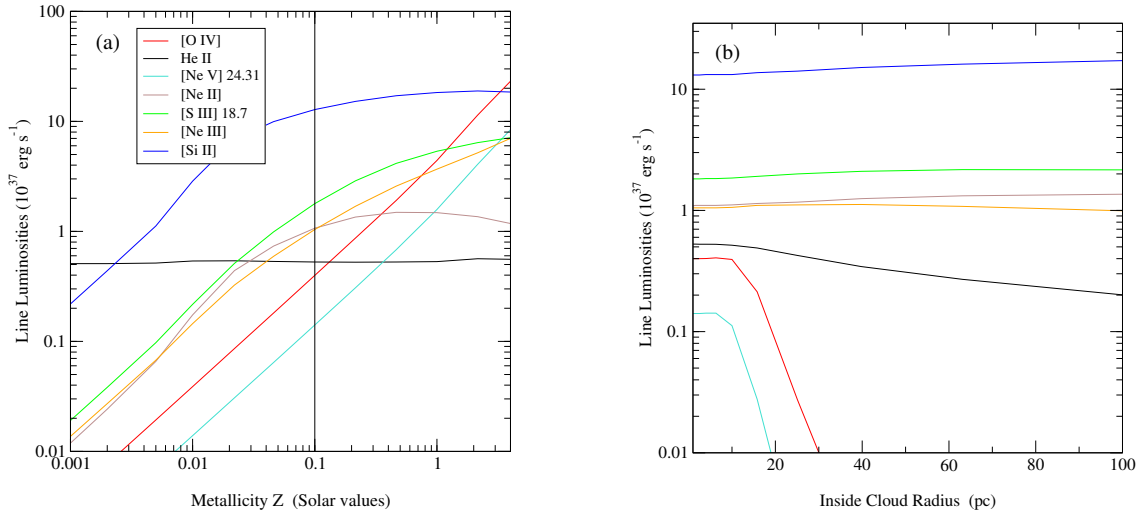


Fig. 7.— The dependence of the simulated lines from CLOUDY on: a) Cloud metallicity. b) The inner radius of the cloud. The vertical line marks the base model value of $Z = 0.1 Z_{\odot}$. The line colors are the same but only labeled in the left panel.

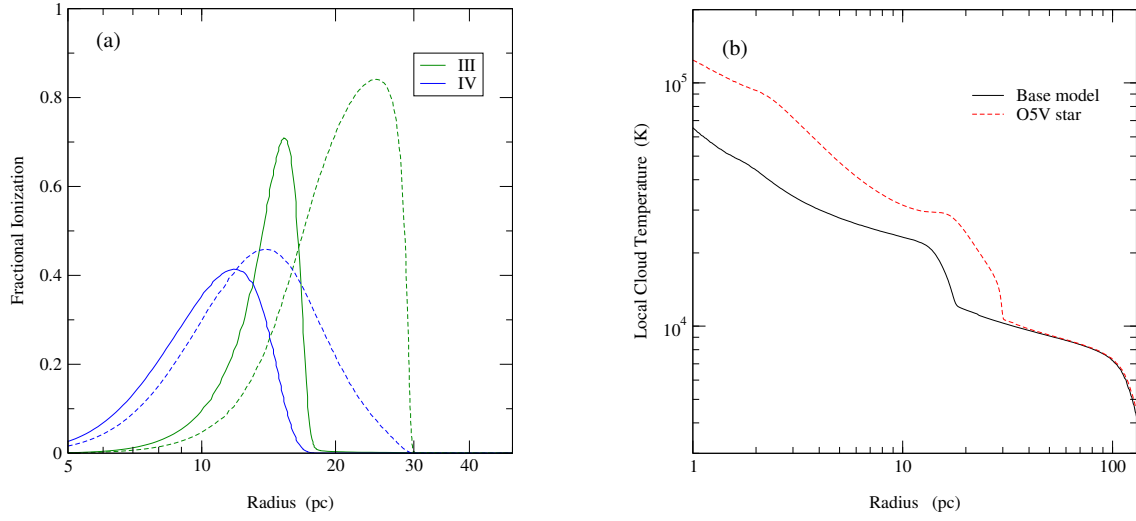


Fig. 8.— Comparison between the base model, with the B2Ib star (continuous line) and the model with the O5V star (dashed line). a) The oxygen ionic structure in the cloud (O²⁺ and O³⁺). b) Local temperature in the cloud.

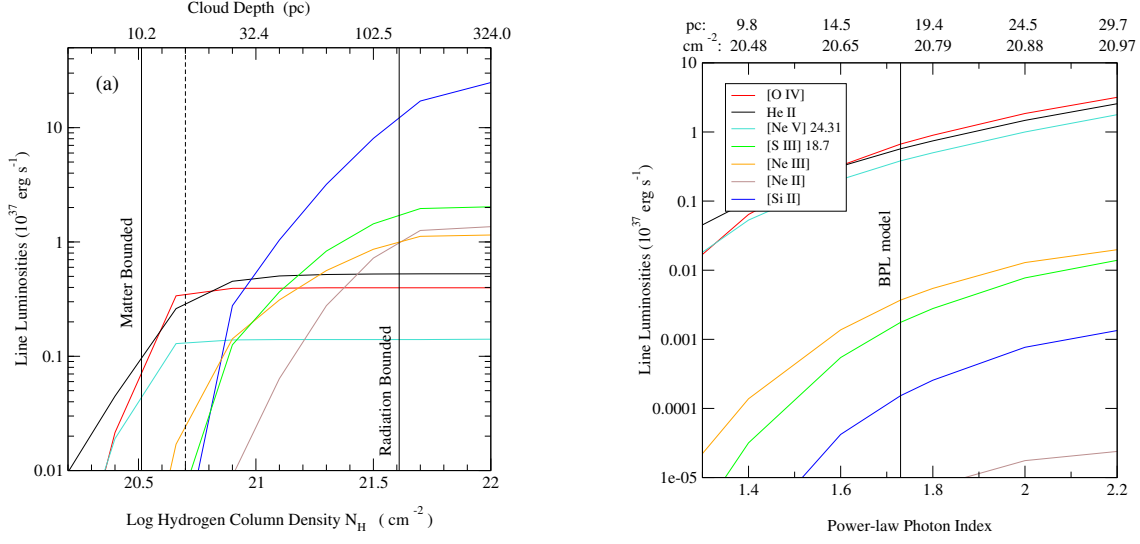


Fig. 9.— This figure illustrates the difference between a matter bounded and radiation bounded nebula. The line colors are only labeled in the right panel. a) The dependence of the simulated lines from CLOUDY on the cloud hydrogen column density for the base model. The equivalent depth of the spherical cloud is also marked on the top X-axis. Both vertical continuous lines mark the column density for the base model, but one value was obtained by fitting the X-ray data with the base model (matter bounded nebula), while the other is the column in the CLOUDY simulation where the local temperature reached 4000 K (radiation bounded). We also marked with a vertical dashed line the limit where the predictions for the high excitation lines are still compatible with observations. b) The simulated lines using the family of broken power-law models fitted to the X-ray data. The best fit broken PL model (BPL) is marked by the vertical line. The bottom X-axis shows the low-energy photon index for the models. On the top X-axis we mark the corresponding log column densities (lower values) and cloud thickness (upper values). All these models are matter-bounded.

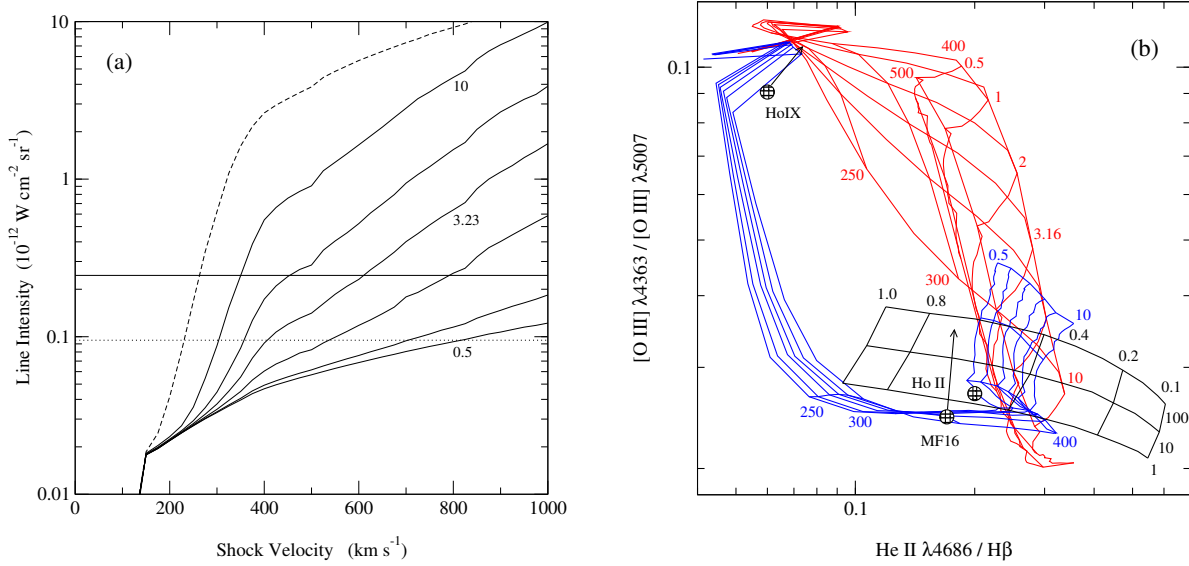


Fig. 10.— Mappings III shocks and ionization models. The shock grids are plotted for magnetic parameters: 0.5, 1, 2, 3.23, 5 and 10 $\mu\text{G cm}^{3/2}$ and for shock velocities 125, 250, 300, 400, 500, 700 and 1000 km s^{-1} . a) [O IV] line intensity shocks predictions. The shocks plus precursor models vary little with the magnetic parameter, and we only show the model with a nominal equipartition value (3.23 $\mu\text{G cm}^{3/2}$, the dashed line). The horizontal lines correspond to the brightest (continuous) and respectively faintest (dotted) pixels in the [O IV] line map in Figure 3 of Paper 1. b) Optical lines diagnostic with shocks and photoionization models. The pure shock models are in red, shocks plus precursor in blue and the photoionization grid in black. For the photoionization grid we varied the density (1, 10 and 100 cm^{-3}), and the inner disk temperature (0.1, 0.2, 0.4, 0.8 and 1.0 keV), and assumed a metallicity of 0.1 Z_{\odot} . For Holmberg IX ULX and MF16 we show with arrows the approximate locations for Solar metallicity. While Holmberg IX ULX is consistent with shocks with modest velocities ($< 100 \text{ km s}^{-1}$), Holmberg II ULX and MF16 seem to require very high velocities. They are however consistent with photoionization.